

RESEARCH ARTICLE

Maximizing Harvested Energy in mmWave IoT Networks: A Tractable Blockage-Aware RIS Framework

JUNGSUN UM¹ AND JAEHYUN PARK^{1b2}, (Member, IEEE)¹Media Broadcasting Research Section, Electronics and Telecommunications Research Institute, Daejeon 34129, South Korea²Department of Electronic Engineering, Pukyong National University, Busan 48513, South Korea

Corresponding author: Jaehyun Park (jaehyun@pknu.ac.kr)

This work was supported in part by the Project for Smart Manufacturing Innovation Research and Development funded Korea Ministry of SMEs and Startups in 2025 under Grant RS-2022-00070516 and in part by the internal fund/grant of Electronics and Telecommunications Research Institute (ETRI) [Development of Fundamental Technology for Next-Generation Media Coding and Transmission Standards] under Grant 26YC1100.

ABSTRACT This paper presents a novel analytical framework for energy harvesting (EH) in Reconfigurable intelligent surface (RIS) assisted mmWave IoT networks under realistic blockage conditions. By leveraging stochastic geometry, we develop a mathematical model that explicitly distinguishes between Line-of-Sight (LoS) and Non-Line-of-Sight (NLoS) propagation based on blockage density. We derive closed-form expressions for the average harvested energy, revealing that RIS deployment significantly mitigates the severe propagation losses caused by urban blockages. Furthermore, we formulate an optimal joint deployment strategy for base stations (BSs) and RISs under budget constraints, proposing an efficient bisection-based algorithm to maximize energy availability. Extensive numerical results validate our analytical framework and demonstrate that strategic RIS deployment is essential for ensuring energy sustainability in dense, blockage-prone mmWave environments.

INDEX TERMS Energy harvesting, reconfigurable intelligent surface, Internet of Things, mmWave, stochastic geometry, blockage modeling.


I. INTRODUCTION

The proliferation of Internet of Things (IoT) devices has created unprecedented challenges in power management and sustainability. With billions of connected devices, the limited battery capacity and difficulty of battery replacement in many deployment scenarios have become critical constraints [1], [2]. Energy harvesting (EH) has emerged as a promising solution, potentially enabling perpetual operation of IoT devices by extracting energy from ambient sources [3]. Among various EH techniques, radio-frequency (RF) energy harvesting has gained significant attention due to its controllability and deployment flexibility [4], [5].

The evolution towards millimeter-wave (mmWave) frequencies (30-300 GHz) for next-generation wireless systems offers unique opportunities and challenges for RF energy harvesting. On one hand, mmWave systems can leverage

higher antenna gains through compact array implementations, potentially enabling more efficient directional energy transfer [6]. On the other hand, mmWave propagation is severely affected by blockages—even a single obstacle can cause complete signal attenuation, making the Line-of-Sight (LoS) condition critical for energy harvesting [7]. This extreme blockage sensitivity, combined with high path loss, significantly reduces energy transfer efficiency in dense urban deployments [8]. These fundamental mmWave propagation characteristics necessitate novel approaches to enhance EH performance in blockage-prone environments.

Reconfigurable intelligent surfaces (RISs) have recently emerged as a revolutionary technology to reshape wireless propagation environments, particularly well-suited for mmWave systems [9], [10], [11]. By dynamically altering the electromagnetic properties of incident signals through programmable reflecting elements, RISs can intelligently redirect mmWave signals around obstacles, creating favorable propagation conditions without additional power

The associate editor coordinating the review of this manuscript and approving it for publication was Byung-Seo Kim .

consumption or complex signal processing [12]. The passive nature of RISs makes them particularly attractive for mmWave frequencies where active relaying would be costly. While RISs have been extensively studied for mmWave communication performance enhancement [10], [13], their potential for improving energy harvesting in mmWave blockage-affected environments remains largely unexplored, particularly from an analytical perspective that captures realistic urban deployment conditions.

Several works have investigated RIS-assisted wireless communications and energy harvesting. In [14], [15], and [16], the authors analyzed RIS-enhanced simultaneous wireless information and power transfer (SWIPT) systems, demonstrating significant performance gains in ideal channel conditions. In [17], RISs are employed to control transmit signal directions to wirelessly power Non-Line-of-Sight (NLoS) devices. This study maximizes the minimum harvested power among all devices in a dual-hop communication scenario. In [18] and [19], the coverage probability and average achievable rate in RIS-assisted large-scale networks are analyzed using stochastic geometry. Authors in [20] and [21] studied RIS-assisted energy harvesting networks using stochastic geometry. However, these works do not explicitly model the impact of blockages, which is a critical limitation for mmWave systems. The work in [22] analyzed coverage probability in RIS-assisted integrated sensing and communication networks using a blockage-aware approach that separates LoS and NLoS conditions. However, it did not address energy harvesting aspects in mmWave environments. Accordingly, the interplay between blockage density, RIS deployment, and energy harvesting performance in mmWave environments lacks rigorous mathematical characterization.

To address these challenges, we propose a novel analytical framework for blockage-aware energy harvesting in RIS-assisted mmWave IoT networks. Our key contributions are:

- We develop a comprehensive system model tailored for mmWave systems. This model explicitly separates network nodes into LoS and NLoS processes based on blockage probability, enabling a more accurate characterization of mmWave urban environments.
- We derive closed-form expressions for the probability distribution of harvested energy in both direct LoS links and RIS-assisted links. These derivations account for the distinct propagation characteristics of each scenario in mmWave bands.
- We analyze the average harvested energy, providing insights into how blockage density—which is particularly severe in mmWave frequencies—influences the performance gain from RIS deployment.
- From the analytic results, we identify optimal RIS deployment strategies for different mmWave urban environments characterized by blockage density and base station (BS)/RIS densities. We provide mathematical proofs and numerical validation for these strategies. Specifically, we discuss the unimodality of the average harvested energy with respect to the RIS density and

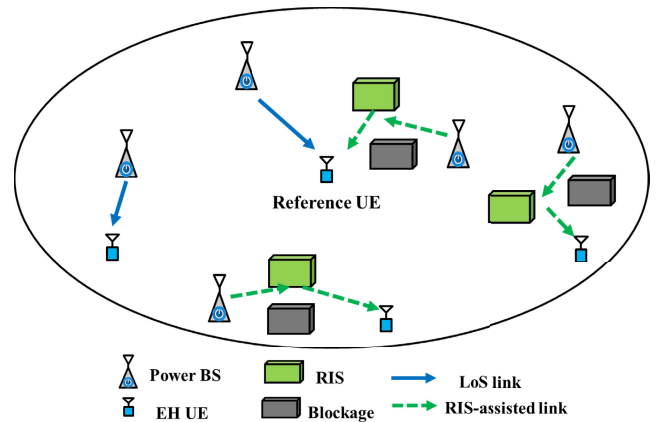


FIGURE 1. System model of the RIS-assisted mmWave IoT network with blockages. The network consists of mmWave power BSs, RISs, EH UEs, and blockages. The solid lines represent LoS links, and the dashed lines represent RIS-assisted links.

propose a bisection method to efficiently find the optimal RIS density.

- We provide comprehensive numerical results that validate our analytical framework. These results demonstrate the significant improvement in energy harvesting performance achievable through strategic RIS deployment in blockage-prone mmWave environments.

The remainder of this paper is organized as follows: Section II presents the mmWave system model and assumptions. Section III establishes the mathematical preliminaries for our analysis. Section IV develops the analytical framework for harvested energy performance. Section V analyzes RIS deployment strategies. Section VI presents numerical results and discussion. Finally, Section VII concludes the paper.

II. SYSTEM MODEL FOR MMWAVE NETWORKS

A. NETWORK TOPOLOGY

We consider a downlink mmWave wireless-powered IoT network where BSs operating in the mmWave band transmit RF signals that can be harvested by IoT devices (referred to as energy harvesting user equipment (EH UE)) as in Fig. 1. The network is enhanced by mmWave-compatible RISs that assist energy transfer, particularly crucial in blockage-prone mmWave environments. Throughout the paper, mmWave BSs are located according to a homogeneous Poisson Point Process (PPP) Φ_B with density λ_B in the 2D plane. Each BS transmits with constant power P_B . RISs designed for mmWave frequencies are also distributed according to a homogeneous PPP Φ_R with density λ_R in the 2D plane. Each RIS consists of M reflecting elements arranged in a uniform planar array, sized appropriately for mmWave wavelengths. Without loss of generality, we focus our analysis on a typical EH UE located at the origin (Slivnyak's theorem [23]). Finally, blockages are modeled as a Boolean scheme of rectangles [22], [24], with average length L and density λ_O . This model leads to a distance-dependent LoS probability function, which is particularly important in mmWave systems

TABLE 1. Summary of key notations.

| Notation | Description |
|--------------------------|---|
| Φ_B, Φ_R | PPPs of BSs and RISs with densities λ_B and λ_R |
| $\Phi_{B,L}, \Phi_{B,N}$ | PPPs of LoS BSs and NLoS BSs |
| β | Blockage density parameter ($\beta = \lambda_O L$ in (1)) |
| $p_{LoS}(d)$ | LoS probability at distance d ($e^{-\beta d}$) |
| α_L, α_N | Path loss exponents for LoS and NLoS links |
| C_L, C_N | Path loss intercepts at reference distance (1 m) |
| m_L, m_N | Nakagami- m fading parameters |
| P_B | BS transmit power |
| M | Number of reflecting elements |
| η | RIS reflection efficiency factor |
| G_{RIS} | RIS passive beamforming gain (ηM^2) |
| R_L | Random variable (RV) for distance to the nearest LoS BS |
| R_R | RV for distance to the nearest RIS |
| R_{RN} | RV for distance from nearest RIS to nearest NLoS BS |
| ζ | Energy conversion efficiency |
| $P_{H,L}, P_{H,R}$ | Harvested power from LoS and RIS-assisted links |

due to their high sensitivity to obstacles. Key mathematical notations used throughout this paper are summarized in Table 1.

B. MMWAVE CHANNEL AND PROPAGATION MODEL

We incorporate distinct channel models for LoS and NLoS links, capturing the fundamentally different propagation characteristics in each scenario for mmWave frequencies.

1) MMWAVE PATH LOSS

For a mmWave link of length d , the path loss is modeled as:

- LoS link: $PL_L(d) = C_L d^{-\alpha_L}$
- NLoS link: $PL_N(d) = C_N d^{-\alpha_N}$

where C_L and C_N are the path loss intercepts at a reference distance of 1 meter for LoS and NLoS links, respectively; α_L and α_N are the path loss exponents for LoS and NLoS links, respectively. In mmWave systems, typically $C_N \ll C_L$ (NLoS paths experience significantly higher attenuation) and $\alpha_N > \alpha_L$ (NLoS paths have steeper distance-dependent loss). The large difference between LoS and NLoS path loss in mmWave bands makes the distinction between these two propagation modes particularly critical for energy harvesting performance.

2) SMALL-SCALE FADING

We model small-scale fading using Nakagami- m fading, which is appropriate for mmWave channels:

- LoS links: Nakagami- m fading with parameter m_L , which approaches Rician fading with strong line-of-sight component typical of mmWave LoS channels
- NLoS links: Nakagami- m fading with parameter m_N (typically $m_N = 1$, corresponding to Rayleigh fading for scattered mmWave NLoS paths)

The channel power gain under Nakagami- m fading follows a Gamma distribution with shape parameter m and scale parameter $1/m$.

3) MMWAVE BLOCKAGE MODEL

The presence of blockages severely affects mmWave signal propagation due to the poor diffraction characteristics at high frequencies. Following [22] and [25], the probability that a mmWave link of length d is LoS is given by:

$$p_{LoS}(d) = e^{-\beta d} \tag{1}$$

where $\beta = \lambda_O L$ represents the blockage density parameter, incorporating both the density of obstacles λ_O and their average length L . For mmWave systems, even relatively small obstacles can cause complete blockage, making the blockage parameter β a critical system parameter.¹ Consequently, the probability of NLoS is $p_{NLoS}(d) = 1 - p_{LoS}(d) = 1 - e^{-\beta d}$.

C. RIS MODEL AND OPERATION

Each RIS consists of M passive reflecting elements that can be configured to modify the phase of incident mmWave signals to enhance signal propagation toward the intended receiver. For analytical tractability, we consider the following model and assumptions:

1) RIS REFLECTION

The reflection coefficient of the i -th element is denoted as $\Gamma_i = e^{j\theta_i}$, where $\theta_i \in [0, 2\pi)$ is the phase shift introduced by the element. We assume that phase shifts can be optimally adjusted based on channel state information. In mmWave systems, the small wavelength allows for compact RIS designs with many elements in a small area.

2) RIS GAIN

When phase shifts are optimally configured, the RIS provides a passive beamforming gain. For a RIS with M elements and optimal phase configuration, the effective power gain is modeled as $G_{RIS} = \eta M^2$, where $\eta \in (0, 1]$ is an efficiency factor accounting for practical implementation limitations [27]. The quadratic scaling with the number of elements makes large RIS arrays particularly attractive for mmWave energy harvesting.

3) LINK MODEL

For a mmWave BS-RIS-UE link, the end-to-end channel includes:

- BS-RIS link of length r_{BR}
- RIS-UE link of length r_{RU}
- Corresponding path loss and fading for each link segment
- RIS reflection gain

For analytical tractability, we make the following assumption:

¹We note that the exponential blockage formula in (1) is widely used in stochastic geometry, effectively capturing the macroscopic impact of blockage density. Although real-world obstacles (e.g., buildings) may induce spatial correlation, modeling such effects typically requires complex germ-grain models that preclude tractable analytical derivations [26]. Importantly, our framework remains extensible to correlated scenarios by replacing $p_{LoS}(d)$ with empirical or fit-based probability functions that implicitly capture these correlation effects.

Assumption 1: BS-RIS and RIS-UE links are assumed to be LoS with high probability, as RISs are typically deployed at elevated positions with lower blockage probability. This assumption is commonly adopted in RIS analysis [28] and is particularly reasonable for mmWave systems where RISs can be strategically placed on building facades or rooftops to maintain LoS paths.

D. ENERGY HARVESTING SCENARIOS IN MMWAVE

The typical EH UE in mmWave networks harvests energy through one of the following mutually exclusive scenarios:

- **Direct LoS EH:** The UE harvests energy directly from the strongest LoS BS, typically the nearest one. In mmWave systems, this scenario provides the highest harvested energy due to favorable LoS propagation.
- **RIS-assisted EH for NLoS BS-UE:** When direct LoS links to BSs are unavailable or blocked (a common situation in mmWave due to high blockage sensitivity), the UE harvests energy via the strongest RIS-assisted path. In this scenario, we consider the strongest BS-RIS-UE link where the BS-UE direct link is NLoS. This scenario is particularly important in mmWave networks where blockages are frequent.

Accordingly, the UE harvests energy exclusively from either a direct BS link or an RIS-assisted link.

For analytical tractability, and considering that IoT devices typically operate in the low-power regime (below saturation), we use the following linearized model:

$$P_H = \zeta P_{rx}, \quad (2)$$

where $\zeta \in (0, 1]$ is the energy conversion efficiency [29].

III. POINT PROCESS CHARACTERIZATION AND LINK ANALYSIS

This section establishes the mathematical foundation for analyzing the energy harvesting performance in mmWave networks. We characterize the distribution of network nodes under blockage effects and derive key statistical properties of the mmWave links.

A. BLOCKAGE-AWARE POINT PROCESSES FOR mmWave

Due to the presence of blockages—particularly severe in mmWave systems—we need to distinguish between LoS and NLoS BSs with respect to the typical UE. We apply the concept of location-dependent thinning to the original BS PPP. Given the original mmWave BS process Φ_B with intensity λ_B , the LoS BS process $\Phi_{B,L}$ and NLoS BS process $\Phi_{B,N}$ with respect to the typical UE at the origin are defined through location-dependent thinning:

- $\Phi_{B,L} = \{x \in \Phi_B : \text{link from } x \text{ to origin is LoS}\}$
- $\Phi_{B,N} = \{x \in \Phi_B : \text{link from } x \text{ to origin is NLoS}\}$

These processes have the following properties:

Lemma 1: The LoS BS process $\Phi_{B,L}$ is a non-homogeneous PPP with intensity function:

$$\lambda_{B,L}(r) = \lambda_B e^{-\beta r}. \quad (3)$$

Similarly, the NLoS BS process $\Phi_{B,N}$ is a non-homogeneous PPP with intensity function:

$$\lambda_{B,N}(r) = \lambda_B (1 - e^{-\beta r}). \quad (4)$$

Proof: We apply the location-dependent thinning theorem for Poisson point processes [23]. Given a homogeneous PPP Φ with constant intensity λ , when each point $x \in \Phi$ is independently retained with probability $p(x)$ and deleted with probability $1 - p(x)$, the resulting point process is a non-homogeneous PPP with intensity function $\lambda'(x) = \lambda p(x)$.

For the LoS BS process $\Phi_{B,L}$, a point at distance r from the origin is retained with probability $p_{LoS}(r) = e^{-\beta r}$ as defined in our blockage model. Therefore, applying the thinning theorem, we obtain the intensity function:

$$\lambda_{B,L}(r) = \lambda_B \cdot p_{LoS}(r) = \lambda_B e^{-\beta r} \quad (5)$$

Similarly, for the NLoS BS process $\Phi_{B,N}$, a point at distance r is retained with probability $p_{NLoS}(r) = 1 - e^{-\beta r}$. By the same thinning theorem, the intensity function is:

$$\lambda_{B,N}(r) = \lambda_B \cdot p_{NLoS}(r) = \lambda_B (1 - e^{-\beta r}) \quad (6)$$

The independence of the thinning operation across different points ensures that both $\Phi_{B,L}$ and $\Phi_{B,N}$ inherit the Poisson property from the original process Φ_B . \square

B. DISTANCE DISTRIBUTIONS TO NEAREST POINTS

We now derive the distributions of distances from the typical UE to the nearest LoS BS and nearest RIS, which will be essential for our energy harvesting analysis in mmWave networks.

Lemma 2: Let R_L denote the distance from the typical UE to its nearest LoS BS. The cumulative distribution function (CDF) of R_L is:

$$\begin{aligned} F_{R_L}(r) &= 1 - \exp\left(-2\pi\lambda_B \int_0^r t e^{-\beta t} dt\right), \\ &= 1 - \exp\left(-\frac{2\pi\lambda_B}{\beta^2} [1 - e^{-\beta r} (1 + \beta r)]\right). \end{aligned} \quad (7)$$

The probability density function (PDF) is:

$$f_{R_L}(r) = 2\pi\lambda_B r e^{-\beta r} \exp\left(-\frac{2\pi\lambda_B}{\beta^2} [1 - e^{-\beta r} (1 + \beta r)]\right). \quad (8)$$

Proof: For a non-homogeneous PPP with intensity function $\lambda(r)$, the fundamental void probability theorem states that the probability of having no points in a bounded Borel set $B \subset \mathbb{R}^2$ is:

$$\mathbb{P}(\text{No points in } B) = \exp\left(-\int_B \lambda(x) dx\right). \quad (9)$$

The CDF of the distance R_L to the nearest point is:

$$\begin{aligned} F_{R_L}(r) &= \mathbb{P}(R_L \leq r) \\ &= 1 - \mathbb{P}(R_L > r) \\ &= 1 - \mathbb{P}(\text{No points of } \Phi_{B,L} \text{ in } B(0, r)) \end{aligned} \quad (10)$$

where $B(0, r)$ is a ball (disk in \mathbb{R}^2) of radius r centered at the origin.

Applying the void probability theorem with the intensity function $\lambda_{B,L}(t) = \lambda_B e^{-\beta t}$ from Lemma 1:

$$F_{R_L}(r) = 1 - \exp\left(-\int_{B(0,r)} \lambda_{B,L}(t) dt\right). \quad (11)$$

Converting to polar coordinates (t, θ) , we have:

$$\begin{aligned} \int_{B(0,r)} \lambda_{B,L}(t) dt &= \int_0^r \int_0^{2\pi} \lambda_B e^{-\beta t} t d\theta dt \\ &= 2\pi \lambda_B \int_0^r t e^{-\beta t} dt. \end{aligned} \quad (12)$$

Therefore:

$$F_{R_L}(r) = 1 - \exp\left(-2\pi \lambda_B \int_0^r t e^{-\beta t} dt\right), \quad (13)$$

and, after integration by parts with $u = t$ and $dv = e^{-\beta t} dt$, we get (7). To derive the PDF, we differentiate the CDF with respect to r , resulting in (8). \square

Lemma 3: Let R_R denote the distance from the typical UE to its nearest RIS. The CDF and PDF of R_R are:

$$F_{R_R}(r) = 1 - e^{-\pi \lambda_R r^2} \quad (14)$$

$$f_{R_R}(r) = 2\pi \lambda_R r e^{-\pi \lambda_R r^2} \quad (15)$$

Proof: Since RISs are distributed according to a homogeneous PPP Φ_R with constant intensity λ_R , we can directly apply standard results from PPP theory [23]. \square

Lemma 4: Let R_{RN} denote the distance from the nearest RIS (to the typical UE) to its nearest NLoS BS. Given that the nearest RIS is located at distance r_R from the UE, we can approximate the conditional CDF of R_{RN} by assuming local homogeneity for the NLoS BS process.

The effective density of NLoS BSs in the vicinity of the RIS at distance r_R is $\lambda_N^{eff}(r_R) = \lambda_B(1 - e^{-\beta r_R})$. The conditional CDF of R_{RN} is then approximated as:

$$F_{R_{RN}|r_R}(r) \approx 1 - \exp\left(-\pi \lambda_B(1 - e^{-\beta r_R})r^2\right) \quad (16)$$

The corresponding conditional PDF is:

$$f_{R_{RN}|r_R}(r) \approx 2\pi \lambda_B(1 - e^{-\beta r_R})r \exp\left(-\pi \lambda_B(1 - e^{-\beta r_R})r^2\right) \quad (17)$$

Proof: The NLoS BS process $\Phi_{B,N}$ is an inhomogeneous PPP with intensity $\lambda_{B,N}(y) = \lambda_B(1 - e^{-\beta \|y\|})$, which depends on the distance from the origin (the typical UE).

To find the distribution of the distance from the nearest RIS (at location z with $\|z\| = r_R$) to the nearest point in $\Phi_{B,N}$, we would need to solve the integral $\Lambda(r_R, r) = \int_{B(z,r)} \lambda_{B,N}(y) dy$, which has no simple closed-form solution.

To obtain a tractable result, we introduce a common and effective approximation. We assume that for the purpose of finding the nearest NLoS BS to the RIS at location z , the intensity of the NLoS BS process is approximately constant in the local neighborhood of z . We approximate the intensity

at any point y near z with the intensity evaluated at z , i.e., $\lambda_{B,N}(y) \approx \lambda_{B,N}(z)$.

Since $\|z\| = r_R$, this gives an effective homogeneous density:

$$\lambda_N^{eff}(r_R) = \lambda_B(1 - e^{-\beta r_R}) \quad (18)$$

With this local homogeneity assumption, the NLoS BS process in the vicinity of the RIS is treated as a homogeneous PPP with density $\lambda_N^{eff}(r_R)$. The distance R to the nearest point in a homogeneous PPP with density λ is given by the well-known void probability formula:

$$\begin{aligned} F_R(r) &= 1 - \mathbb{P}(\text{No points in disk of radius } r) \\ &= 1 - \exp(-\lambda \cdot \text{Area}(B(0, r))) \\ &= 1 - \exp(-\lambda \pi r^2) \end{aligned} \quad (19)$$

Substituting $\lambda = \lambda_N^{eff}(r_R)$, we obtain the approximate conditional CDF in (16). Differentiating this with respect to r yields the conditional PDF in (17). This approximation accurately captures the dependence on the RIS's location r_R . \square

C. CHANNEL GAIN DISTRIBUTIONS

We derive the distributions of channel gains for both direct and RIS-assisted mmWave links.

Lemma 5: The channel power gain G_L for a LoS link of length r follows a Gamma distribution with shape parameter m_L and scale parameter $\frac{C_L r^{-\alpha_L}}{m_L}$. Its PDF is:

$$f_{G_L|r}(g) = \frac{m_L^{m_L}}{\Gamma(m_L)} \left(\frac{1}{C_L r^{-\alpha_L}}\right)^{m_L} g^{m_L-1} e^{-\frac{m_L g}{C_L r^{-\alpha_L}}}, \quad (20)$$

where $\Gamma(m_L)$ is the gamma function.

Proof: Under Nakagami- m fading with parameter m_L , the channel amplitude follows a Nakagami distribution. Consequently, the channel power gain, which is the square of the amplitude, follows a Gamma distribution. For a Nakagami- m fading channel with parameter m_L , the channel power gain G_L follows a Gamma distribution with shape parameter $k = m_L$ and scale parameter $\theta = \frac{\Omega}{m_L}$, where Ω is the mean power gain. In our model, with path loss, the mean power gain at distance r is $\Omega = C_L r^{-\alpha_L}$. Therefore, the scale parameter is $\theta = \frac{C_L r^{-\alpha_L}}{m_L}$, resulting in the PDF of (20). \square

Lemma 6: For a RIS-assisted mmWave link with BS-RIS distance r_{BR} and RIS-UE distance r_{RU} , when optimal phase shifts are applied, the end-to-end channel gain G_R can be approximated as:

$$G_R \approx \eta M^2 C_L^2 (r_{BR} r_{RU})^{-\alpha_L} G_{BR} G_{RU}, \quad (21)$$

where G_{BR} and G_{RU} are the fading power gains of the BS-RIS and RIS-UE links, respectively, which follow Gamma distributions with shape parameters m_L and scale parameters $1/m_L$.

Proof: Consider the cascaded mmWave channel from BS to UE via the RIS. Under Assumption 1, both BS-RIS

and RIS-UE links are LoS. The channel from BS to RIS can be modeled as:

$$\mathbf{h}_{BR} = \sqrt{C_L r_{BR}^{-\alpha_L} G_{BR}} \cdot \mathbf{a}(\theta_{BR}, \phi_{BR}), \quad (22)$$

where $\mathbf{a}(\theta_{BR}, \phi_{BR})$ is the array response vector at the RIS for the incident direction from the BS, r_{BR} is the BS-RIS distance, and G_{BR} is the fading power gain. Similarly, the channel from RIS to UE is:

$$\mathbf{h}_{RU} = \sqrt{C_L r_{RU}^{-\alpha_L} G_{RU}} \cdot \mathbf{a}(\theta_{RU}, \phi_{RU}). \quad (23)$$

With a RIS having M elements, the phase shift matrix can be represented as $\Phi = \text{diag}(e^{j\phi_1}, e^{j\phi_2}, \dots, e^{j\phi_M})$, where ϕ_i is the phase shift of the i -th element. The end-to-end channel gain is:

$$G_R = |(\mathbf{h}_{RU})^H \Phi \mathbf{h}_{BR}|^2. \quad (24)$$

With optimal phase configuration, the phases ϕ_i are set to cancel the phases of the individual channel components, maximizing the combined gain. Taking into account practical implementation efficiency η , the maximum achievable gain is:

$$\begin{aligned} G_R &\approx \eta M^2 \cdot C_L r_{BR}^{-\alpha_L} G_{BR} \cdot C_L r_{RU}^{-\alpha_L} G_{RU} \\ &= \eta M^2 C_L^2 (r_{BR} r_{RU})^{-\alpha_L} G_{BR} G_{RU}. \end{aligned} \quad (25)$$

The factor M^2 arises from the coherent combining of signals across all M elements when phases are perfectly aligned [27]. Under Nakagami- m fading with parameter m_L for both links, G_{BR} and G_{RU} follow Gamma distributions with shape parameter m_L and scale parameter $1/m_L$ (for unit mean power). \square

Remark 1: While the theoretical gain of an RIS scales with M^2 under continuous phase shifting and perfect channel estimation, practical deployments face several hardware limitations. First, phase quantization errors arise from the use of discrete phase shifters (e.g., 1-bit or 2-bit control), which can reduce the beamforming gain by approximately 3-4 dB compared to the ideal case. Second, mutual coupling between closely spaced elements (typically $\lambda/2$) can distort the reflection pattern and reduce efficiency. Third, channel estimation errors in the BS-RIS-UE cascaded link inevitably lead to phase misalignment. In our analytical framework, these cumulative degradation factors are captured by the efficiency factor $\eta \in (0, 1]$ in (21).

IV. ENERGY HARVESTING PERFORMANCE ANALYSIS

In this section, we analyze the energy harvesting performance for both direct LoS and RIS-assisted scenarios in mmWave networks, and then characterize the overall system performance.

From Lemma 2, we first derive the energy harvested from direct LoS BSs analytically and have the following theorem as:

Theorem 1: The average harvested power from the strongest LoS BS in mmWave systems is:

$$\mathbb{E}[P_{H,L}] = \zeta P_B C_L \mathbb{E}[G_L R_L^{-\alpha_L}] = \zeta P_B C_L \int_0^\infty r^{-\alpha_L} f_{R_L}(r) dr. \quad (26)$$

For Nakagami- m fading with parameter m_L and mean channel gain 1 (i.e., $\mathbb{E}[G_L] = 1$):

$$\begin{aligned} \mathbb{E}[P_{H,L}] &= \zeta P_B C_L \int_0^\infty r^{-\alpha_L} f_{R_L}(r) dr \\ &= 2\pi \zeta P_B C_L \lambda_B \int_0^\infty r^{1-\alpha_L} e^{-\beta r} \\ &\quad \cdot \exp\left(-\frac{2\pi \lambda_B}{\beta^2} [1 - e^{-\beta r} (1 + \beta r)]\right) dr. \end{aligned} \quad (27)$$

Next, we analyze the energy harvested through RIS-assisted links when direct LoS links are unavailable—a particularly important scenario in blockage-prone mmWave environments.

Theorem 2: The average harvested power from the strongest RIS-assisted link in mmWave systems is given by applying the law of total expectation over the distribution of the nearest RIS distance:

$$\mathbb{E}[P_{H,R}] = \zeta P_B \eta M^2 C_L^2 \int_0^\infty r_R^{-\alpha_L} \cdot \mathbb{E}[R_{RN}^{-\alpha_L} | R_R = r_R] \cdot f_{R_R}(r_R) dr_R, \quad (28)$$

where $f_{R_R}(r_R) = 2\pi \lambda_R r_R e^{-\pi \lambda_R r_R^2}$ is the PDF of the nearest RIS distance from Lemma 3, and $\mathbb{E}[R_{RN}^{-\alpha_L} | R_R = r_R]$ is the conditional expectation of the inverse path loss from the nearest NLoS BS to the RIS, given the RIS is at distance r_R from the UE. This conditional expectation is calculated using the conditional PDF from Lemma 4:

$$\mathbb{E}[R_{RN}^{-\alpha_L} | R_R = r_R] = \int_0^\infty r_{RN}^{-\alpha_L} f_{R_{RN}|r_R}(r_{RN}) dr_{RN}, \quad (29)$$

where $f_{R_{RN}|r_R}(r_{RN})$ is given by (17).

Proof: The harvested power from the RIS-assisted mmWave link can be expressed as:

$$P_{H,R} = \zeta P_B \eta M^2 C_L^2 (R_R \cdot R_{RN})^{-\alpha_L} G_{BR} G_{RU}, \quad (30)$$

where R_R is the distance from UE to the nearest RIS, R_{RN} is the distance from that RIS to its nearest NLoS BS, and G_{BR}, G_{RU} are the respective fading gains. Using the law of total expectation by conditioning on the nearest RIS distance:

$$\begin{aligned} \mathbb{E}[P_{H,R}] &= \mathbb{E}_{R_R} [\mathbb{E}[P_{H,R} | R_R = r_R]] \\ &= \int_0^\infty \mathbb{E}[P_{H,R} | R_R = r_R] f_{R_R}(r_R) dr_R. \end{aligned} \quad (31)$$

Given $R_R = r_R$, from (25), the conditional expectation becomes:

$$\begin{aligned} \mathbb{E}[P_{H,R} | R_R = r_R] &= \zeta P_B \eta M^2 C_L^2 r_R^{-\alpha_L} \mathbb{E}[R_{RN}^{-\alpha_L} | R_R = r_R] \\ &\quad \cdot \mathbb{E}[G_{BR} G_{RU}]. \end{aligned} \quad (32)$$

Since the fading gains are independent and normalized to unit mean, $\mathbb{E}[G_{BR} G_{RU}] = \mathbb{E}[G_{BR}] \mathbb{E}[G_{RU}] = 1$. The conditional

expectation $\mathbb{E}[R_{RN}^{-\alpha_L} | R_R = r_R]$ is computed using the conditional PDF from Lemma 4:

$$\mathbb{E}[R_{RN}^{-\alpha_L} | R_R = r_R] = \int_0^\infty r_{RN}^{-\alpha_L} f_{R_{RN}|r_R}(r_{RN}) dr_{RN}. \quad (33)$$

Substituting back into the total expectation:

$$\begin{aligned} \mathbb{E}[P_{H,R}] &= \int_0^\infty \zeta P_B \eta M^2 C_L^2 r_R^{-\alpha_L} \mathbb{E}[R_{RN}^{-\alpha_L} | R_R = r_R] f_{R_R}(r_R) dr_R \\ &= \zeta P_B \eta M^2 C_L^2 \int_0^\infty r_R^{-\alpha_L} \mathbb{E}[R_{RN}^{-\alpha_L} | R_R = r_R] f_{R_R}(r_R) dr_R. \end{aligned} \quad (34)$$

This integral must be evaluated numerically, as both the conditional expectation and the outer integral do not have closed-form solutions for general values of α_N and β . \square

Remark 2: (Refinement of the Local Homogeneity Approximation) The local homogeneity approximation used in Theorem 2, while providing a tractable and insightful model, has a subtle limitation. It assumes that the effective density of NLoS BSs, $\lambda_{eff}(r_R)$, is constant within the search region around a RIS located at distance r_R . In reality, the true NLoS density $\lambda_{B,N}(y) = \lambda_B(1 - e^{-\beta\|y\|})$ continues to vary with the distance from the origin (the UE). This discrepancy can introduce a minor systematic bias, as the average density within the search disk around the RIS is slightly different from the density at the RIS's exact location. To further enhance the model's fidelity, especially in regimes where the NLoS density changes rapidly (e.g., low β), a calibration of the effective density can be employed. The key idea is to adjust the effective density based on a predicted search radius, while ensuring the correction does not become physically unrealistic. The procedure is as follows:

- 1) First, an initial estimate of the average BS-RIS distance, \bar{r}_{br} , is calculated using the local homogeneity approximation: $\bar{r}_{br} = 1/(2\sqrt{\lambda_{eff}(r_R)})$.
- 2) A damping factor is computed to limit the influence of the correction when the predicted search radius is excessively large compared to the network's characteristic length scale, $L_{char} = 1/(2\sqrt{\lambda_B})$. The damping factor is given by $\mathcal{D} = \exp(-K_c \bar{r}_{br}/L_{char})$, where $K_{c,1}$ is a pre-defined constant. A calibrated effective distance, r_{eff} , is then calculated by applying the damped correction to the RIS's position: $r_{eff} = r_R + (K_{c,2} \cdot \bar{r}_{br}) \cdot \mathcal{D}$. The term $K_{c,2} \cdot \bar{r}_{br}$ approximates the centroid of the search area.
- 3) The final expectation is calculated using a calibrated effective density, $\lambda_{eff,cal} = \lambda_B(1 - e^{-\beta r_{eff}})$.

This refined model in Remark 1, while more complex, more accurately captures the spatial non-uniformity of the NLoS BS process, leading to a closer match between theoretical predictions and simulation results across a wider range of system parameters.

A. OVERALL ENERGY HARVESTING PERFORMANCE

We now characterize the overall energy harvesting performance in mmWave systems, considering both direct LoS and RIS-assisted scenarios. Specifically, in practical systems, the

typical UE harvests energy from either the strongest LoS BS or the RIS-assisted link, whichever provides higher power. The total harvested power is given by:

$$P_{H,total} = \max(P_{H,L}, P_{H,R}). \quad (35)$$

The following theorem characterizes the overall energy harvesting performance, considering both direct LoS and RIS-assisted scenarios.

Theorem 3: The average overall harvested power in mmWave systems can be approximated as

$$\mathbb{E}[P_{H,total}] = \mathbb{E}[\max(P_{H,L}, P_{H,R})] \approx \mathbb{E}[P_{H,L}] + \mathbb{E}[P_{H,R}]. \quad (36)$$

Proof: Because $P_{H,L}, P_{H,R} \geq 0$,

$$\begin{aligned} \mathbb{E}[\max(P_{H,L}, P_{H,R})] \\ = \mathbb{E}[P_{H,L}] + \mathbb{E}[P_{H,R}] - \mathbb{E}[\min(P_{H,L}, P_{H,R})]. \end{aligned} \quad (37)$$

We note that LoS and RIS scenarios are largely mutually exclusive due to the blockage model—particularly true in mmWave systems where blockages cause severe signal attenuation. Specifically, when β is low, UE tends to find LoS BSs with a small distance, inducing large $\mathbb{E}[P_{H,L}]$, and hardly finds NLoS BSs with a low effective NLoS BS node density. Therefore, RIS relays weak power signal to UE. When β is high, UE hardly finds LoS BSs with a small distance, inducing small $\mathbb{E}[P_{H,L}]$, resulting in $P_{H,R} \gg P_{H,L}$. Therefore, $\mathbb{E}[\min(P_{H,L}, P_{H,R})] \approx 0$ and the probability that both LoS and RIS provide substantial power simultaneously is low, making $\mathbb{E}[P_{H,L}] + \mathbb{E}[P_{H,R}]$ a tight approximation for $\mathbb{E}[\max(P_{H,L}, P_{H,R})]$. \square

V. RIS DEPLOYMENT STRATEGY

Based on the energy harvesting performance analysis, we propose the optimal RIS deployment strategy to maximize the harvested energy under blockage-prone mmWave environments. Specifically, to determine the optimal deployment strategy under a budget constraint, we aim to find the densities $(\lambda_B^*, \lambda_R^*)$ that maximize the total average harvested energy $\mathbb{E}[P_{H,total}]$.

The optimization problem is formulated as follows:

$$\max_{\lambda_B, \lambda_R} \mathbb{E}[P_{H,L}](\lambda_B, \beta) + \mathbb{E}[P_{H,R}](\lambda_B, \lambda_R, \beta) \quad (38)$$

$$\text{s.t. } \lambda_B + \gamma \lambda_R = \Lambda, \quad (39)$$

$$\lambda_B \geq 0, \lambda_R \geq 0 \quad (40)$$

where Λ is the total deployment budget and γ is the relative cost factor of a RIS compared to a BS. We note that, from Theorems 1 and 2, $\mathbb{E}[P_{H,L}](\lambda_B, \beta)$ and $\mathbb{E}[P_{H,R}](\lambda_B, \lambda_R, \beta)$ in the objective function involve numerical integrations. Accordingly, we propose a numerical optimization approach.

Using the budget constraint (39), we express λ_B as a function of λ_R :

$$\lambda_B(\lambda_R) = \Lambda - \gamma \lambda_R. \quad (41)$$

The feasible range for λ_R is thus $[0, \Lambda/\gamma]$. The objective function becomes a function of λ_R only:

$$f(\lambda_R) = \mathbb{E}[P_{H,L}](\lambda_B(\lambda_R), \beta) + \mathbb{E}[P_{H,R}](\lambda_B(\lambda_R), \lambda_R, \beta). \quad (42)$$

Therefore, for a given blockage density β , we find the optimal RIS density λ_R^* by solving:

$$\lambda_R^* = \arg \max_{0 \leq \lambda_R \leq \Lambda/\gamma} f(\lambda_R). \quad (43)$$

The following proposition provides a useful insight into efficiently finding the optimal RIS density.

Proposition 1: Let $f(\lambda_R)$ denote the total average harvested energy as a function of λ_R in (42). The function $f(\lambda_R)$ is unimodal with respect to λ_R over the feasible domain $0 \leq \lambda_R \leq \Lambda/\gamma$. Consequently, there exists a unique optimal RIS density λ_R^* that maximizes the harvested energy.

Proof: 1) *Boundary Analysis:* At the lower boundary $\lambda_R = 0$, the network consists solely of BSs with maximum density $\lambda_B = \Lambda$. In this regime, $\mathbb{E}[P_{H,L}] > 0$ and $\mathbb{E}[P_{H,R}] = 0$, so $f(0) > 0$. At the upper boundary $\lambda_R = \Lambda/\gamma$, the BS density approaches zero ($\lambda_B = 0$). Since the harvested energy in passive networks fundamentally requires RF sources, both $\mathbb{E}[P_{H,L}]$ and $\mathbb{E}[P_{H,R}]$ vanish. Thus, $f(\Lambda/\gamma) = 0$.

2) *Marginal Trade-off Analysis:* Let us consider the derivative $\frac{df}{d\lambda_R} \approx \frac{\partial \mathbb{E}[P_{H,R}]}{\partial \lambda_R} - \gamma \left| \frac{\partial \mathbb{E}[P_{H,L}]}{\partial \lambda_B} \right|$. In the sparse RIS regime ($\lambda_R \rightarrow 0^+$), the introduction of RISs provides new energy harvesting paths for NLoS users who were previously in outage. Since the direct LoS energy $\mathbb{E}[P_{H,L}]$ saturates at high λ_B , the marginal gain from adding RIS diversity typically exceeds the marginal loss from slightly reducing λ_B . Therefore, the slope is positive ($\frac{df}{d\lambda_R} > 0$) at the beginning. Conversely, in the dense RIS regime ($\lambda_R \rightarrow \Lambda/\gamma$), the scarcity of energy sources (BSs) becomes the bottleneck. Reducing λ_B further causes a rapid decay in total energy, outweighing any gain from additional RISs. Thus, the slope becomes negative ($\frac{df}{d\lambda_R} < 0$) as it approaches the upper bound.

Since $\mathcal{P}(\lambda_R)$ is a sum of continuous, smooth functions (involving exponential and power-law terms characteristic of PPPs) and exhibits a transition from a positive slope to a negative slope over the domain, it possesses a unique global maximum λ_R^* . \square

From Proposition 1, the function, $f(\lambda_R)$, increases from the left endpoint and decreases towards the right endpoint, implying a single peak in between and it is also confirmed numerically in Fig. 7. Given this unimodal property, we can use the bisection method to find the optimal λ_R^* , efficiently. The algorithm searches for the point where $\frac{df(\lambda_R)}{d\lambda_R} = 0$, which is summarized in Algorithm 1. The derivative computation in line 4 of Algorithm 1 can be approximated numerically as:

$$\frac{df(\lambda_R)}{d\lambda_R} \approx \frac{f(\lambda_R + h) - f(\lambda_R - h)}{2h}, \quad (44)$$

where h is a small constant. Once λ_R^* is found, the optimal BS density is determined as $\lambda_B^* = \Lambda - \gamma \lambda_R^*$.

Algorithm 1 Bisection Algorithm for Optimal λ_R

Require: System parameters: $\Lambda, \gamma, \beta, P_B, M$, tolerance ϵ
Ensure: Optimal number of beams λ_R^*

- 1: Initialize: $a \leftarrow 0, b \leftarrow \Lambda/\gamma$
- 2: **while** $b - a > \epsilon$ **do**
- 3: $c \leftarrow \lfloor (a + b)/2 \rfloor$
- 4: Compute $f'(c) = \left. \frac{df(\lambda_R)}{d\lambda_R} \right|_{\lambda_R=c}$
- 5: **if** $f'(c) > 0$ **then**
- 6: $a \leftarrow c$ ▷ Optimum is in the right half
- 7: **else**
- 8: $b \leftarrow c$ ▷ Optimum is in the left half
- 9: **end if**
- 10: **end while**
- 11: $\lambda_R^* \leftarrow \lfloor (a + b)/2 \rfloor$ **return** λ_R^*

The proposed optimization framework offers a direct pathway for network planning. In practice, operators should first estimate the blockage parameter β based on local building statistics. Next, the relative cost factor γ is determined by the ratio of the total cost of ownership between an RIS and a BS. Using these inputs, Algorithm 1 computes the optimal RIS density λ_R^* . Our analysis suggests a clear strategic direction: in low-blockage regimes ($\beta < 0.05$), resources should be prioritized for BS densification to maximize direct LoS connectivity. Conversely, in dense urban environments ($\beta > 0.05$) or when RISs are cost-effective ($\gamma < 0.2$), shifting the budget toward RIS deployment significantly enhances energy coverage by mitigating blockage effects.

VI. NUMERICAL RESULTS AND DISCUSSION

In this section, we validate our analytical results through extensive Monte Carlo simulations and provide insights into the energy harvesting performance of RIS-assisted mmWave IoT networks under different blockage conditions. We generate multiple realizations of BS and RIS spatial distributions according to homogeneous PPPs with the corresponding densities. The blockage effect is modeled by location-dependent thinning of the BS process as described in Section II. All simulations were conducted over a square area of $500m \times 500m$. Unless otherwise specified, the default parameters used in our mmWave simulations are summarized in Table 1.

Fig. 2 shows the CDF of the distance to the nearest LoS BS for different blockage densities in mmWave systems. The solid lines represent the theoretical results from Lemma 2, while the dashed lines show the empirical CDFs from simulations. We observe an exact match between theory and simulation, confirming the accuracy of our distance distribution analysis in Lemma 2. As the blockage density β increases, the distance to the nearest LoS BS tends to increase, which agrees with our intuition that higher blockage density—particularly severe in mmWave—reduces the likelihood of having nearby LoS BSs and shifts the CDF curve to the right.

TABLE 2. mmWave system simulation parameters.

| Parameter | Value |
|--|--|
| Carrier frequency f_c | 28 GHz |
| BS density λ_B | 1×10^{-4} BSs/m ² |
| RIS density λ_R | 2.5×10^{-3} RISs/m ² |
| BS transmit power P_B | 43 dBm (20W) |
| LoS path loss exponent α_L | 2.1 |
| NLoS path loss exponent α_N | 4.0 |
| LoS path loss intercept C_L | -20 dB |
| NLoS path loss intercept C_N | -36 dB |
| Nakagami fading parameter for LoS m_L | 3 |
| Nakagami fading parameter for NLoS m_N | 1 |
| Number of RIS elements M | {80, 100} |
| RIS efficiency factor η | 0.8 |
| Energy conversion efficiency ζ | 0.7 |

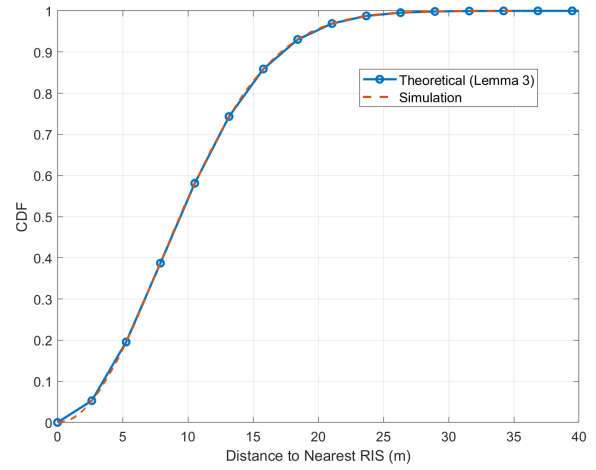


FIGURE 3. CDF of distance to nearest RIS.

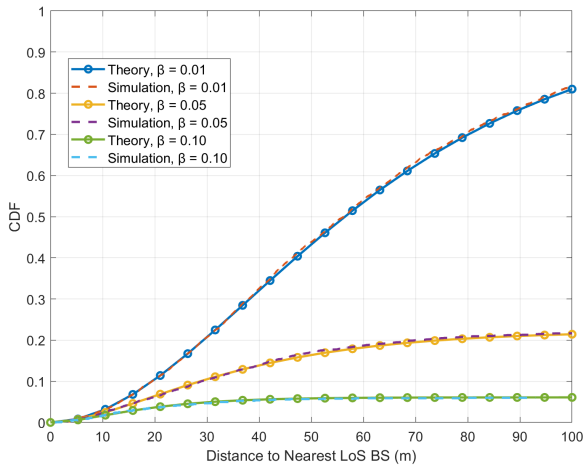


FIGURE 2. CDF of distance to nearest LoS BS for different blockage densities β in mmWave systems.

Fig. 3 validates Lemma 3 by comparing the theoretical and simulated CDFs of the distance to the nearest RIS. Again, we observe a strong agreement between theory and simulation, confirming the accuracy of our analysis. Since RISs form a homogeneous PPP without thinning due to blockages, the distribution follows the standard result for the nearest neighbor in a 2D PPP.

Fig. 4 shows the distribution of channel gains for a LoS link at a fixed distance of 100 meters. The theoretical distribution follows a Gamma distribution as derived in Lemma 5. The histogram from Monte Carlo simulations closely matches the theoretical PDF, validating our channel gain model.

In Fig. 5, the average RIS-assisted harvested energy is evaluated when the basic local homogeneity approximation in (18) and the proposed calibrated model in Remark 2 are utilized. Here, we have used the refined model for the NLoS BS density in Remark 2 with $(K_{c,1}, K_{c,2}) = (0.1, 0.05)$. As shown in the figure, at low blockage density ($\beta \approx 0.01$), the basic approximation underestimates the energy. In contrast, our calibrated model reduces this error, closely matching the simulation results across the entire range of β .

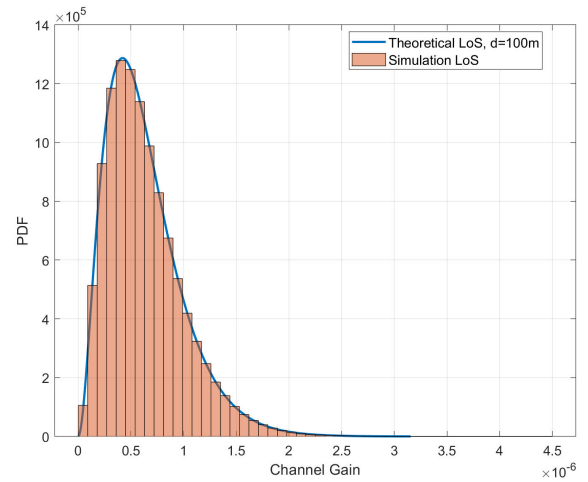


FIGURE 4. Distribution of channel gain for mmWave LoS link at distance 100m.

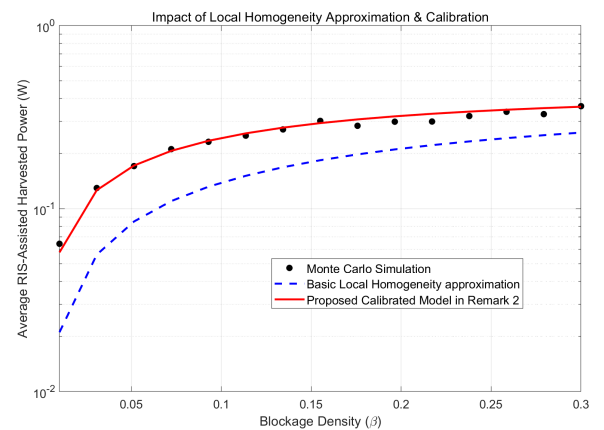


FIGURE 5. Average RIS-assisted harvested energy vs. blockage density: Monte Carlo simulation, basic local homogeneity approximation in (18), and the proposed calibrated model in Remark 2.

This confirms that the calibration effectively compensates for the spatial inhomogeneity of the NLoS BS process.

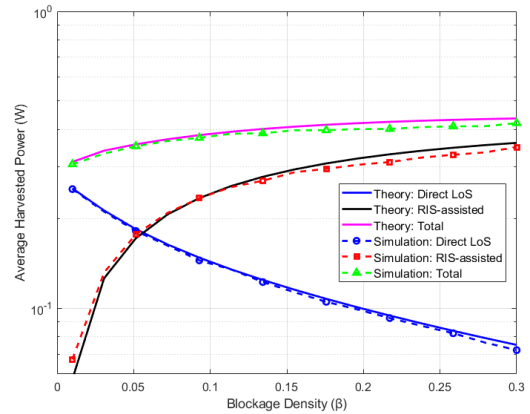
Fig. 6 (a) and (b) present the average harvested energy as a function of blockage density in mmWave systems,

comparing direct LoS, RIS-assisted, and total harvested energy for $M = \{80, 100\}$, respectively. The total harvested energy represents the practical scenario where the UE selects the maximum power between LoS and RIS-assisted links, i.e., $P_{H,\text{total}} = \max(P_{H,L}, P_{H,R})$. The solid lines represent the theoretical results, while the dashed lines with markers show the simulation results. As derived in Theorem 3, the approximation $\mathbb{E}[P_{H,\text{total}}] \approx \mathbb{E}[P_{H,L}] + \mathbb{E}[P_{H,R}]$ in (36) is highly accurate because LoS and RIS scenarios are largely mutually exclusive due to the blockage model—particularly true in mmWave where blockages cause severe attenuation. In addition, as the blockage density increases, the energy from direct LoS link decreases, while the energy from RIS-assisted link increases. That is, the relative contribution of RIS-assisted energy harvesting to overall performance increases for a large β . This is because, as blockage density β increases, the probability of having a LoS BS decreases. This demonstrates that in mmWave environments with high blockage density, RIS deployment becomes increasingly important for maintaining energy harvesting performance. More specifically, in Fig. 6 (a), we observe a distinct crossover point at approximately $\beta \approx 0.05$. Beyond this threshold, the network enters an RIS-dominant regime where the RIS-assisted link provides up to $3.2\times$ more energy than the direct LoS link at $\beta = 0.2$. This quantitatively confirms that in dense urban environments (high β), relying solely on BS densification is less effective than deploying RISs. Interestingly, when M is large, the energy harvesting performance can be further improved through the RIS deployment.

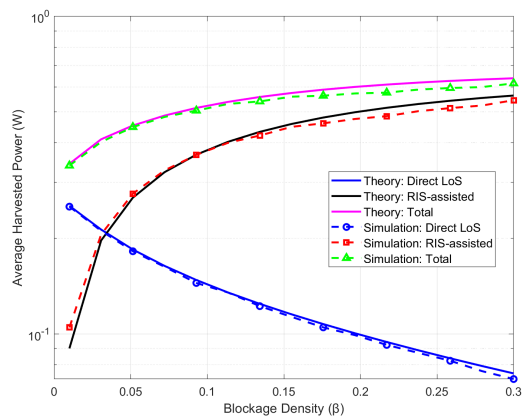
Fig. 7 presents the average harvested energy as a function of blockage density in mmWave systems for $m_L = 6$ and $M = 80$. It can be found that the crossover point between LoS and RIS-dominant regimes shifts negligibly compared to Fig. 6 (a). That is, our key insights are robust to the specific choice of fading parameters.

Fig. 8 investigates the core problem of our proposed RIS deployment strategy from Section V, illustrating the average harvested energy as a function of the RIS density λ_R under a fixed total deployment budget $\Lambda = 0.003$ and blockage density $\beta = 0.05$ in mmWave systems. The two subfigures correspond to RISs with $M = 80$ and $M = 100$ elements, respectively. From the figures, the average harvested energy is concave with respect to λ_R , as discussed in Section V. Each plot shows curves for different relative cost factors γ , which dictates the trade-off between deploying BSs and RISs ($\lambda_B = \Lambda - \gamma\lambda_R$).

The results clearly validate our theoretical framework, demonstrating that for each cost factor γ , there exists a unique optimal RIS density λ_R^* that maximizes the harvested energy. As predicted by our model, when the relative cost of RISs (γ) increases, the optimal strategy shifts towards deploying fewer RISs (i.e., the peak of the curve moves to the left). This is because a higher γ makes each RIS deployment consume a larger portion of the budget, which would otherwise be used for deploying BSs. Furthermore, comparing Fig. 8(a) and (b), we observe that increasing the number of RIS elements M not



(a)



(b)

FIGURE 6. Average harvested energy vs. blockage density in mmWave systems, comparing direct LoS, RIS-assisted, and total harvested energy for (a) $M = 80$ and (b) $M = 100$. Here, Nakagami fading parameter for LoS (m_L) is set as 3.

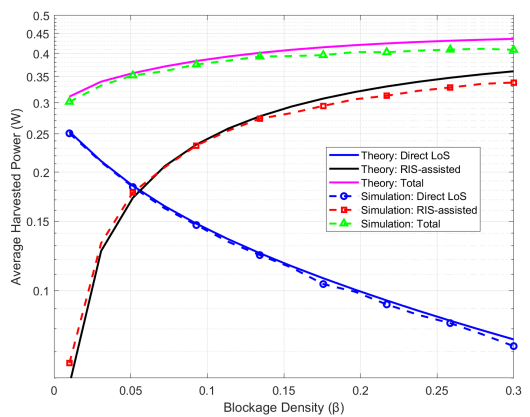
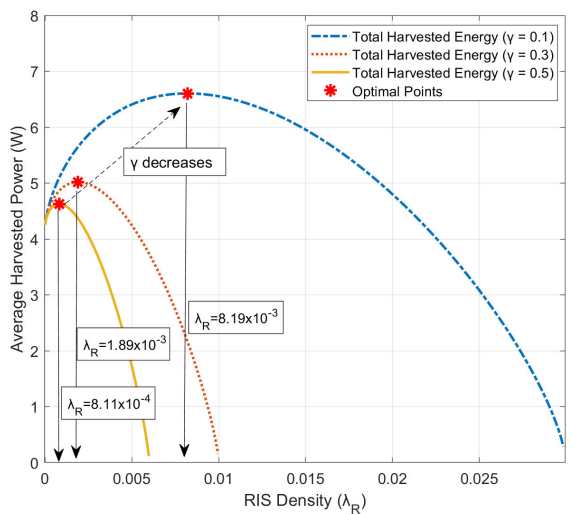
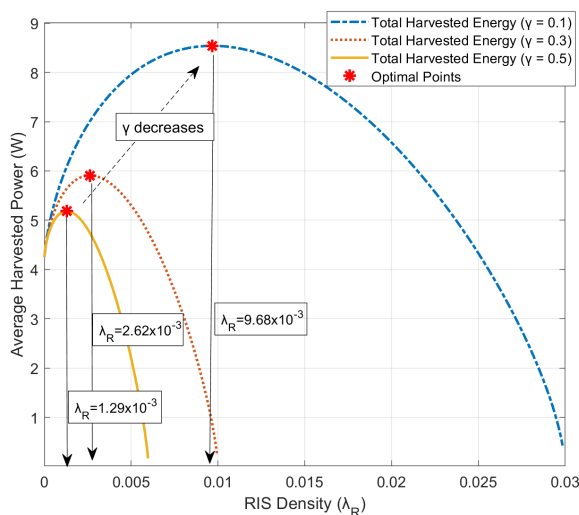


FIGURE 7. Average harvested energy vs. blockage density in mmWave systems, comparing direct LoS, RIS-assisted, and total harvested energy for $m_L = 6$ and $M = 80$.

only significantly boosts the overall harvested energy but also increases the optimal RIS density λ_R^* . This implies that when RISs are more powerful (larger M), it is more beneficial to allocate a larger portion of the deployment budget to them.



(a)



(b)

FIGURE 8. Average harvested energy vs. RIS density (λ_R) in mmWave systems for (a) $M = 80$ and (b) $M = 100$ when $\gamma = \{0.1, 0.3, 0.5\}$, $\Lambda = 0.003$, and $\beta = 0.05$.

In Fig. 8, the performance at $\lambda_R = 0$ corresponds to the baseline ‘conventional mmWave IoT network’ where only mmWave BSs serve as RF energy sources ($\lambda_B = \Lambda$). By comparing the peak energy at the optimal λ_R^* with this baseline, we observe that the proposed RIS-assisted deployment yields approximately 40% higher average harvested energy than the traditional RIS-free topology for $\gamma = 0.1$ and $M = 100$. This confirms that simply densifying mmWave BSs is less cost-effective than integrating RISs in blockage-prone IoT environments. In addition, it is noteworthy that the harvested energy curves highlight the importance of precise dimensioning, especially for lower cost factors ($\gamma = 0.1$). A deviation from the optimal λ_R^* leads to a noticeable reduction in energy efficiency, necessitating the proposed algorithm to ensure cost-effective network planning.

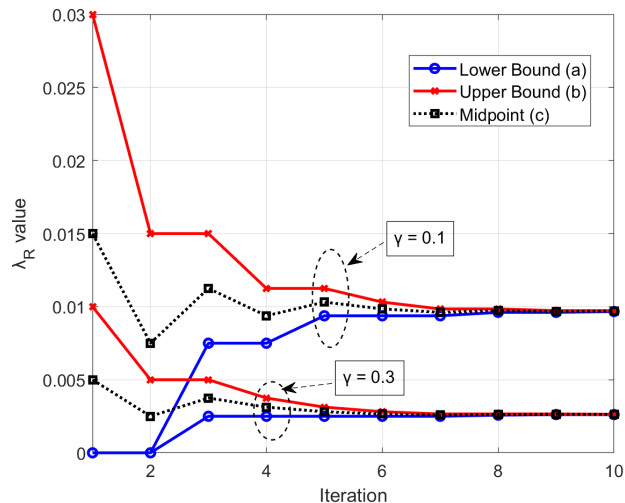


FIGURE 9. RIS density (λ_R) over iterations in Algorithm 1 for $\gamma = \{0.1, 0.3\}$ with $\Lambda = 0.003$ and $\beta = 0.05$ in mmWave systems.

Fig. 9 demonstrates the convergence of our proposed bisection-based optimization, Algorithm 1, for finding the optimal RIS density λ_R^* . The figure shows that the algorithm converges rapidly to a stable value for different cost factors. For a lower relative cost ($\gamma = 0.1$), the algorithm converges to a higher optimal RIS density compared to the case with a higher cost ($\gamma = 0.3$). This result is perfectly aligned with the findings from Fig. 8 and confirms that our proposed algorithm provides a reliable and efficient method for determining the optimal deployment strategy in practical mmWave scenarios.

VII. CONCLUSION

In this paper, we established a comprehensive stochastic geometry framework for analyzing energy harvesting performance in RIS-assisted mmWave IoT networks under realistic blockage conditions. By modeling the network with location-dependent thinning of PPPs, we successfully distinguished between LoS and NLoS links and derived analytical expressions for the average harvested energy. Our analysis revealed that the additive approximation of LoS and RIS-assisted energy is highly accurate in mmWave environments due to the strong mutual exclusivity of propagation paths across different blockage regimes. The results quantified the critical role of RISs, showing that they become the dominant energy source as blockage density increases, effectively mitigating the high susceptibility of mmWave signals to obstacles.

A key contribution of this work is the rigorous formulation of an optimal deployment strategy for BSs and RISs under budget constraints. We proved the unimodality of the total average harvested energy function with respect to RIS density and proposed the bisection-based optimization algorithm to efficiently find the optimal RIS density. Our numerical results, validated by extensive Monte Carlo simulations, demonstrate that a unique optimal deployment mix exists and is highly sensitive to the relative cost (γ) and array size (M) of the RISs. Specifically, we showed that for cost-effective

RISs (low γ) or large-scale arrays (high M), shifting resources toward RIS deployment significantly enhances energy sustainability.

This framework not only provides practical design guidelines for network operators but also serves as a foundation for future research. Promising extensions include investigating multi-RIS coordination for cooperative beamforming, incorporating dynamic blockage models for mobile users, and exploring the trade-offs in RIS-assisted SWIPT networks.

REFERENCES

- [1] D. D. Wentzloff, A. Alghaihab, J. Im, O. Abdelatty, and T. Odelberg, "Ultralow-power receivers: Overcoming battery limitations to facilitate self-powered operation," *IEEE Solid State Circuits Mag.*, vol. 13, no. 3, pp. 33–37, Summer, 2021.
- [2] M. A. Albreem, A. M. Sheikh, M. J. K. Bashir, and A. A. El-Saleh, "Towards green Internet of Things (IoT) for a sustainable future in Gulf cooperation council countries: Current practices, challenges and future prospective," *Wireless Netw.*, vol. 29, no. 2, pp. 539–567, Feb. 2023.
- [3] S. Sudevalayam and P. Kulkarni, "Energy harvesting sensor nodes: Survey and implications," *IEEE Commun. Surveys Tuts.*, vol. 13, no. 3, pp. 443–461, 3rd Quart., 2011.
- [4] X. Lu, P. Wang, D. Niyato, D. I. Kim, and Z. Han, "Wireless networks with RF energy harvesting: A contemporary survey," *IEEE Commun. Surveys Tuts.*, vol. 17, no. 2, pp. 757–789, 2nd Quart., 2015.
- [5] B. Clerckx, R. Zhang, R. Schober, D. W. K. Ng, D. I. Kim, and H. V. Poor, "Fundamentals of wireless information and power transfer: From RF energy harvester models to signal and system designs," *IEEE J. Sel. Areas Commun.*, vol. 37, no. 1, pp. 4–33, Jan. 2019.
- [6] Y. Niu, Y. Li, D. Jin, L. Su, and A. V. Vasilakos, "A survey of millimeter wave communications (mmWave) for 5G: Opportunities and challenges," *Wireless Netw.*, vol. 21, no. 8, pp. 2657–2676, Nov. 2015.
- [7] A. N. Uwaechia and N. M. Mahyuddin, "A comprehensive survey on millimeter wave communications for fifth-generation wireless networks: Feasibility and challenges," *IEEE Access*, vol. 8, pp. 62367–62414, 2020.
- [8] T. Bai, R. Vaze, and R. W. Heath, "Analysis of blockage effects on urban cellular networks," *IEEE Trans. Wireless Commun.*, vol. 13, no. 9, pp. 5070–5083, Sep. 2014.
- [9] C. Huang, S. Hu, G. C. Alexandropoulos, A. Zappone, C. Yuen, R. Zhang, M. D. Renzo, and M. Debbah, "Holographic MIMO surfaces for 6G wireless networks: Opportunities, challenges, and trends," *IEEE Wireless Commun.*, vol. 27, no. 5, pp. 118–125, Oct. 2020.
- [10] X. Yuan, Y.-J.-A. Zhang, Y. Shi, W. Yan, and H. Liu, "Reconfigurable-intelligent-surface empowered wireless communications: Challenges and opportunities," *IEEE Wireless Commun.*, vol. 28, no. 2, pp. 136–143, Apr. 2021.
- [11] S. Hassouna, M. A. Jamshed, J. Rains, J. U. R. Kazim, M. U. Rehman, M. Abualhayja, L. Mohjazi, T. J. Cui, M. A. Imran, and Q. H. Abbasi, "A survey on reconfigurable intelligent surfaces: Wireless communication perspective," *IET Commun.*, vol. 17, no. 5, pp. 497–537, Mar. 2023.
- [12] E. Basar, M. Di Renzo, J. De Rosny, M. Debbah, M.-S. Alouini, and R. Zhang, "Wireless communications through reconfigurable intelligent surfaces," *IEEE Access*, vol. 7, pp. 116753–116773, 2019.
- [13] Q. Wu and R. Zhang, "Towards smart and reconfigurable environment: Intelligent reflecting surface aided wireless network," *IEEE Commun. Mag.*, vol. 58, no. 1, pp. 106–112, Jan. 2020.
- [14] Q. Wu and R. Zhang, "Weighted sum power maximization for intelligent reflecting surface aided SWIPT," *IEEE Wireless Commun. Lett.*, vol. 9, no. 5, pp. 586–590, May 2020.
- [15] B. Zhang, K. Yang, K. Wang, and G. Zhang, "Performance analysis for RIS-assisted SWIPT-enabled IoT systems," *IEEE Trans. Wireless Commun.*, vol. 23, no. 8, pp. 10030–10043, Aug. 2024.
- [16] Y. Wei, Z. Peng, J. Tang, X. Zhang, K.-K. Wong, and J. Chambers, "Max-min fair beamforming design for a RIS-assisted system with SWIPT," *IEEE Trans. Veh. Technol.*, vol. 73, no. 8, pp. 12148–12153, Aug. 2024.
- [17] L. Zhao, Z. Wang, and X. Wang, "Wireless power transfer empowered by reconfigurable intelligent surfaces," *IEEE Syst. J.*, vol. 15, no. 2, pp. 2121–2124, Jun. 2021.
- [18] T. Wang, G. Chen, M.-A. Badiu, and J. P. Coon, "Performance analysis of RIS-assisted large-scale wireless networks using stochastic geometry," *IEEE Trans. Wireless Commun.*, vol. 22, no. 11, pp. 7438–7451, Nov. 2023.
- [19] Y. Xu, C. Huang, L. Wei, Y. Zhu, Z. Yang, J. He, J. Yang, Z. Zhang, C. Yuen, and M. Debbah, "Coverage and rate analysis for distributed RISs-assisted mmWave communications," *IEEE Trans. Wireless Commun.*, vol. 23, no. 10, pp. 15070–15082, Oct. 2024.
- [20] Y. Zheng, S. Bi, Y. J. Zhang, Z. Quan, and H. Wang, "Intelligent reflecting surface enhanced user cooperation in wireless powered communication networks," *IEEE Wireless Commun. Lett.*, vol. 9, no. 6, pp. 901–905, Jun. 2020.
- [21] M. M. Saleh, N. A. Muhammad, N. Seman, and N. I. A. Apandi, "Stochastic geometry analysis of reconfigurable intelligent surface-assisted millimeter-wave energy harvesting networks," *IEEE Access*, vol. 13, pp. 47375–47388, 2025.
- [22] X. Gan, C. Huang, Z. Yang, X. Chen, F. Bader, Z. Zhang, C. Yuen, Y. Liang Guan, and M. Debbah, "Modeling and coverage analysis of RIS-assisted integrated sensing and communication networks," *IEEE Trans. Wireless Commun.*, vol. 24, no. 7, pp. 6006–6019, Jul. 2025.
- [23] M. Haenggi, *Stochastic Geometry for Wireless Networks*. Cambridge, U.K.: Cambridge Univ. Press, 2012.
- [24] T. Bai and R. W. Heath, "Coverage and rate analysis for millimeter-wave cellular networks," *IEEE Trans. Wireless Commun.*, vol. 14, no. 2, pp. 1100–1114, Feb. 2015.
- [25] A. K. Gupta, J. G. Andrews, and R. W. Heath, "On the feasibility of sharing spectrum licenses in mmWave cellular systems," *IEEE Trans. Commun.*, vol. 64, no. 9, pp. 3981–3995, Sep. 2016.
- [26] S. Aditya, H. S. Dhillon, A. F. Molisch, and H. M. Behairy, "A tractable analysis of the blind spot probability in localization networks under correlated blocking," *IEEE Trans. Wireless Commun.*, vol. 17, no. 12, pp. 8150–8164, Dec. 2018.
- [27] W. Tang, M. Z. Chen, X. Chen, J. Y. Dai, Y. Han, M. Di Renzo, Y. Zeng, S. Jin, Q. Cheng, and T. J. Cui, "Wireless communications with reconfigurable intelligent surface: Path loss modeling and experimental measurement," *IEEE Trans. Wireless Commun.*, vol. 20, no. 1, pp. 421–439, Jan. 2021.
- [28] S. Zhang and R. Zhang, "Capacity characterization for intelligent reflecting surface aided MIMO communication," *IEEE J. Sel. Areas Commun.*, vol. 38, no. 8, pp. 1823–1838, Aug. 2020.
- [29] E. Boshkovska, D. W. K. Ng, N. Zlatanov, and R. Schober, "Practical non-linear energy harvesting model and resource allocation for SWIPT systems," *IEEE Commun. Lett.*, vol. 19, no. 12, pp. 2082–2085, Dec. 2015.



JUNGSUN UM received the B.S. and M.S. degrees in electronic and electrical engineering from Sungkyunkwan University, Suwon, Republic of Korea, in 2004 and 2006, respectively, and the Ph.D. degree in electrical engineering from Korea Advanced Institute of Science and Technology, Daejeon, Republic of Korea, in 2017. Since 2006, he has been with the Electronics and Telecommunications Research Institute, Daejeon, where he is currently a Principal Member. His main research interests include spectrum sharing technologies, interference analysis, wireless communication systems, and signal processing for digital television.



JAEHYUN PARK (Member, IEEE) received the B.S. and Ph.D. (M.S. and Ph.D. joint program) degrees in electrical engineering from Korea Advanced Institute of Science and Technology (KAIST), in 2003 and 2010, respectively. From 2010 to 2013, he was a Senior Researcher with the Electronics and Telecommunications Research Institute (ETRI), where he worked on transceiver design and spectrum sensing for cognitive radio systems. From 2013 to 2014,

he was a Postdoctoral Research Associate with the Electrical and Electronic Engineering Department, Imperial College London. He is currently a Professor with the Electronic Engineering Department, Pukyong National University, South Korea. His research interests include signal processing for wireless communications and radar systems, with focus on detection and estimation for MIMO systems, MIMO radar, cognitive radio networks, and joint information and energy transfer.

...